Electronic Supplementary Material (ESI) for Nanoscale.

High Speed, High Temperature Electrical Characterization of Phase Change Materials: Metastable Phases, Crystallization Dynamics, and Resistance Drift

Faruk Dirisaglik,[a] Gokhan Bakan,[a] Zoila Jurado,[a] Sadid Muneer,[a] Mustafa Akbulut,[a] Jonathan Rarey,[a] Lindsay Sullivan,[a] Maren Wennberg,[a] Adrienne King,[a] Lingyi Zhang,[a] Rebecca Nowak,[a] Chung Lam,[b] Helena Silva[a] and Ali Gokirmak[a]

1. Fabricated GST Line Cell Structures

Optical microscope and SEM images of fabricated structures are shown in Figure S1a-f. We have performed highly sensitive 4-point DC measurements using 4-contact devices with similar size to the 2-contact GST line cells (Figure S1g,h). The drift behaviour in amorphous phase is taken into account and the resistivity value is obtained by extrapolation of the 4-point measurement resistances to 1 ms time range (Figure S1i). Comparison between 2-point and 4-point measurements show that there is no significant contact resistances on melt quenched GST line cells. The resistivity values from the AC high-speed and 4-point measurements are also in agreement.

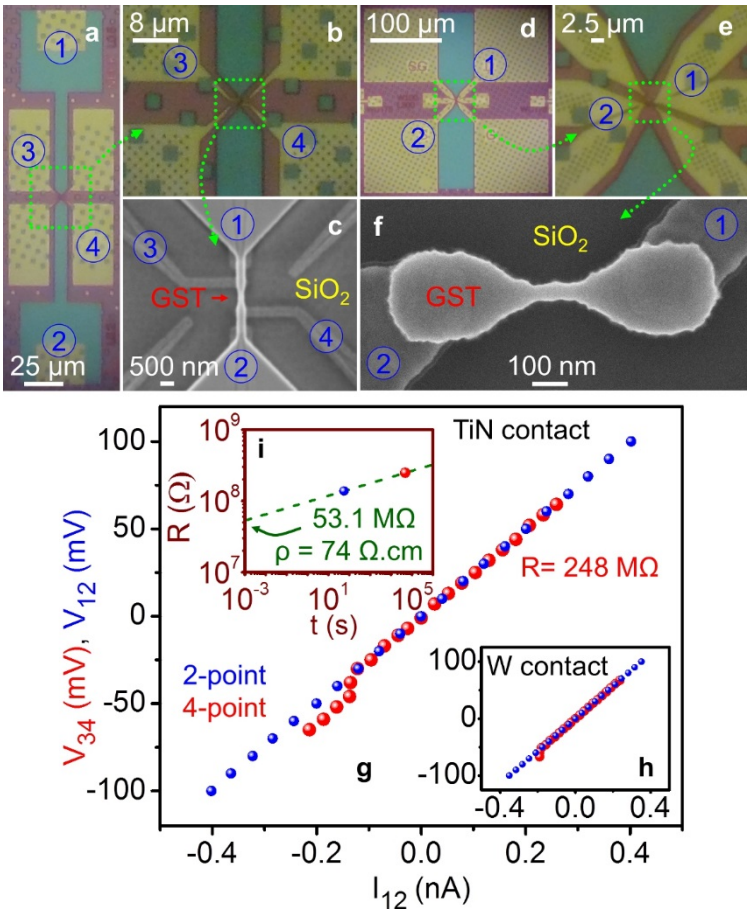

Figure S1. a-f) Optical microscope (a, b, d, e) and SEM (c, f) images of 4 contact (a, b, c) and two contact (d, e, f) devices. g, h) *I-V* characteristics using 4-point (red) and 2-point (blue) DC measurements on devices with TiN contacts (g) and W contacts (h). i) Resistance and resistivity extraction from extrapolation of DC measurements to 1 ms, to take into account the resistance drift in amorphous phase.

2. Measurement Procedure:

GST line cells are annealed at 680 K before each set of pulse measurements; hence all of the samples are in the crystalline (hexagonal) phase for each individual measurement. Electrical measurements consist of 3 main steps:

1) Initial crystalline (hexagonal) cell resistances are measured using 3 methods:
   a) DC current-voltage (*I-V*) sweeps with an Agilent 4156C parameter analyzer (PA) before the high-speed measurement (Figure S2).

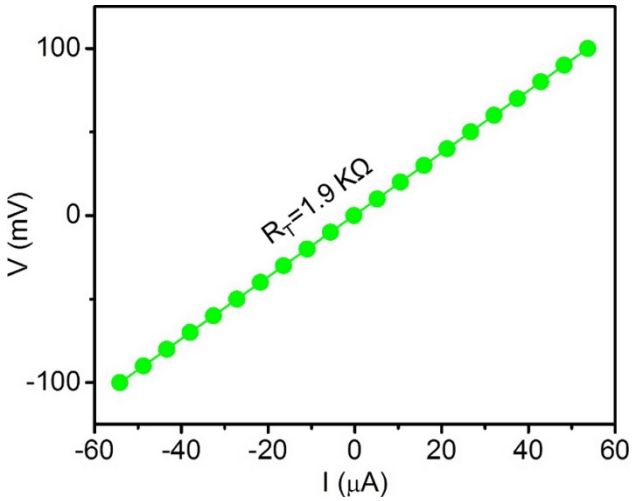

Figure S2. Example *I-V* characteristic based on the DC measurements using the PA to extract initial crystalline (hexagonal) GST line cell. The total resistance (R_T) includes the GST cell resistance (R_{GST}), contact resistance (R_X) (~98 Ω at 500 K), 1 kΩ of load resistance (R_L) and metal extension resistance (R_M) (~200 Ω at 300 K and ~230 Ω at 673 K).

b) A 50 mV baseline voltage applied by a function generator unit (FGU) and the resulting current through the device are measured by a data acquisition (DAQ) card before the high-speed measurement (Figure S3).

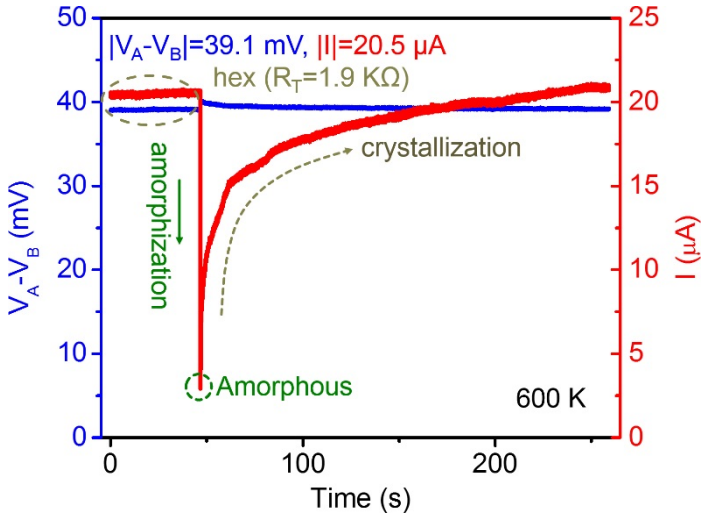

Figure S3. Example of voltage and current acquired by the DAQ card on a crystalline (hexagonal) GST line cell. The total resistance (R_T) includes the GST cell resistance (R_{GST}), contact resistances (R_X) (~98 Ω at 500 K), 1 kΩ of load resistance (R_L) and metal extension resistances (R_M) (~200 Ω at 300 K and ~230 Ω at 673 K).

c) 1 MHz AC segments with amplitudes increasing from 50 mV to 100 mV in 3 steps applied by the FGU during the high-speed measurement. Each amplitude is applied for 26 µs (Figure S4).

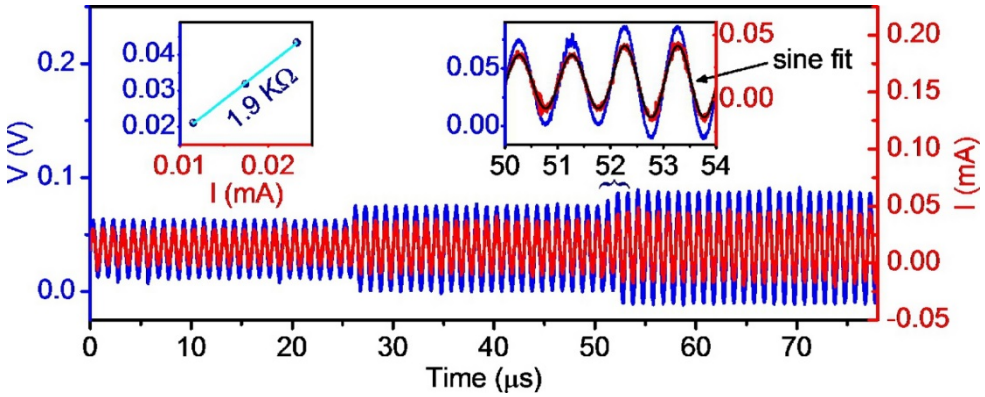

Figure S4. Example of applied and measured electrical signals for a high speed measurement showing voltage and current on a crystalline (hexagonal) GST line cell before the melting pulse). Insets show zoomed-in view of the signals and resistance calculation from the amplitudes of the sinusoidal fits (T_{chuck} = 550 K).

2) Liquid cell resistances are measured during a 1 µs melting pulse with stepwise increasing amplitudes in 8 steps applied by the FGU during the high-speed measurement. Applied pulse amplitudes are chosen based on device dimensions. This pulse is followed by a 0 V bias for 1 µs to cool the cells down to the chuck temperature and amorphize them (Figure S5).

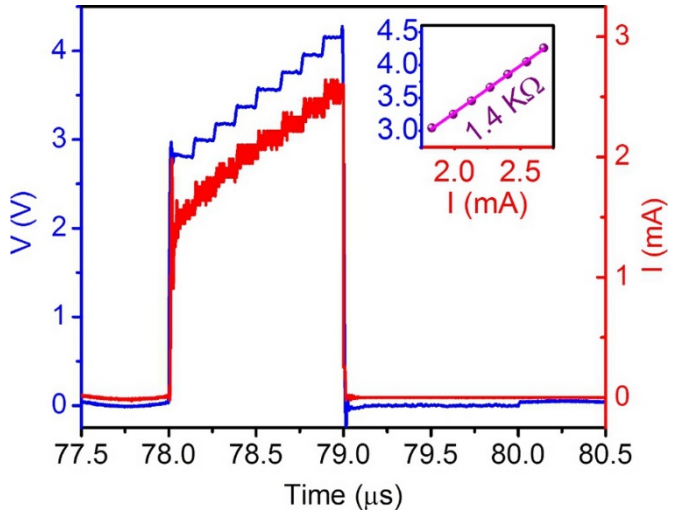

Figure S5. Example of applied and measured electrical signals showing voltage and current on a liquid GST line cell (during pulse). Inset shows the resistance calculation from the linear fits of the amplitudes (T_{chuck} = 550 K).

3) Amorphous cell resistances are measured using:

   a) 1 MHz AC signals with increasing amplitudes from 10 mV to a large value (0.1 to 2.2 V depending on the chuck temperature) in 20 steps and then decreasing amplitudes back to 10 mV in 20 steps applied by the FGU during the high-speed measurements. Each amplitude is applied for 48 μs (Figure S6).

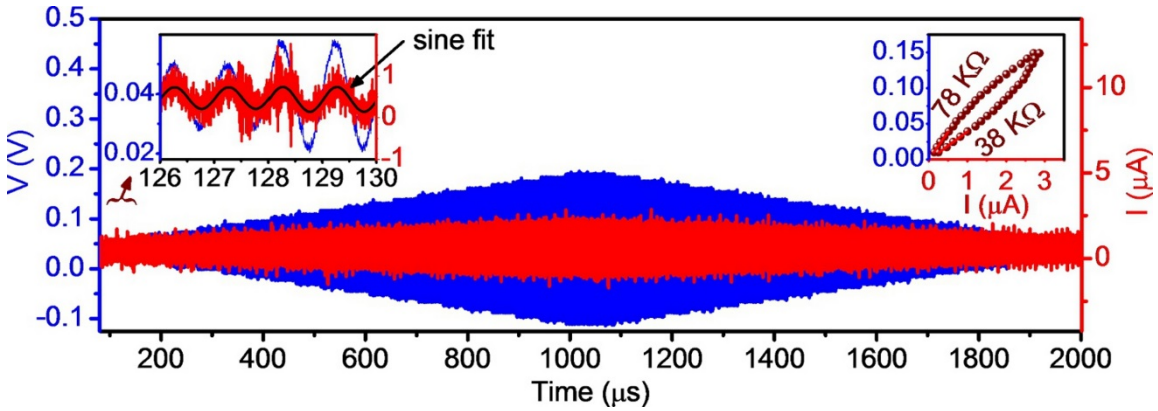

Figure S6. Example of applied and measured electrical signals showing voltage and current on an amorphized GST line cell (after pulse). Insets show zoomed-in view of the signals and resistance calculation from the amplitudes of the sinusoidal fits (T_{chuck} = 550 K).

The amplitudes calculated from the sinusoidal fits are used to construct the *I-V* characteristics (Figure S6 insets) and the resistance values are extracted from the slopes. The amplitude of the AC segments after the pulse are stepped up and then down to check for hysteresis, which would indicate changes in the material during this measurement period (Figure S7).

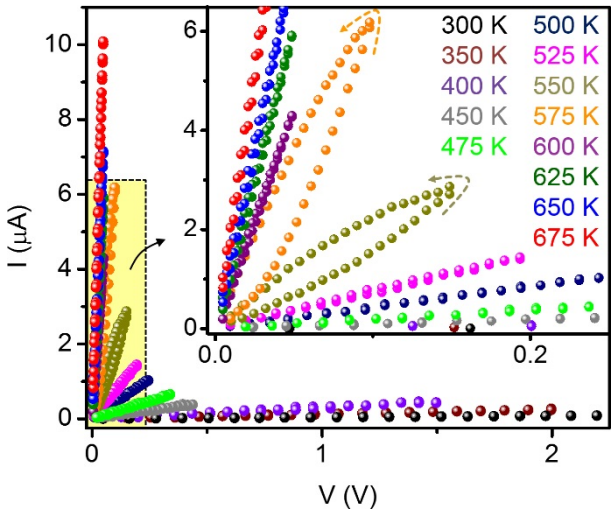

Figure S7. Example *I-V* characteristics based on the high-speed measurements. Inset is the zoomed in view highlighting the hysteresis loops seen for T_{chuck} = ~525-600 K measurements.

b) At low chuck temperatures ($T \leq 400$ K), amorphous cell resistances are also measured using the PA, minutes after the high-speed measurement (Figure S8).

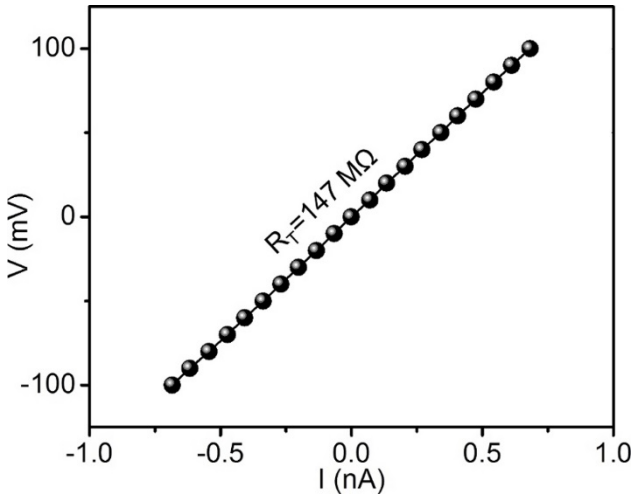

Figure S8. Example *I-V* characteristic based on the DC measurements using the PA to extract amorphous GST line cell resistance. The total resistance (R_T) includes the GST cell resistance (R_{GST}), contact resistances (R_X) (~98 Ω at 500 K), 1 kΩ of load resistance (R_L) and metal extension resistances (R_M) (~200 Ω at 300 K and ~230 Ω at 673 K).

For high chuck temperatures (T ~400-550 K), the amorphized cells transition to crystalline (fcc) over time (~hours). Some of these fcc cell resistances (annealed at 425, 450 and 500 K for ~ hour) are measured using the PA as they are slowly cooled down to 300 K (Figure S9).

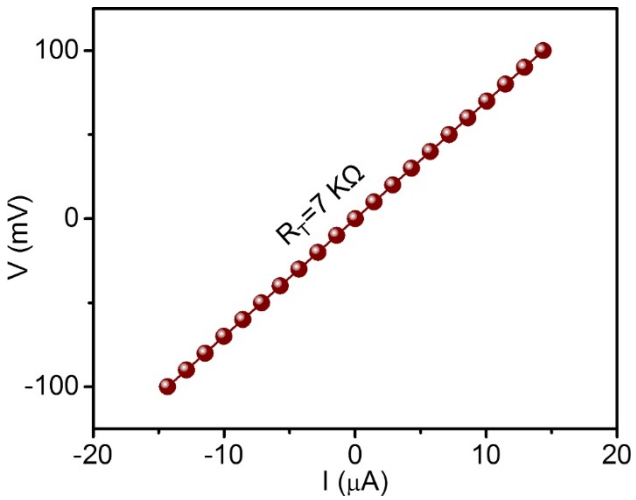

Figure S9. Example *I-V* curve based on the DC measurements using the PA to extract crystalline (fcc) GST line cell resistance. Sample was annealed at 450 K. The total resistance (R_T) includes the GST cell resistance (R_{GST}), contact resistances (R_X) (~98 Ω at 500 K), 1 kΩ of load resistance (R_L) and metal extension resistances (R_M) (~200 Ω at 300 K and ~230 Ω at 675 K).

Slow *R-T* measurements are also performed on an as-fabricated (fcc) cell and two amorphized cells while varying chuck temperature from 300 K to 675 K with 3.5 K/min heating rate and 125 K to 675 K with 1 K/min heating rate using the PA (Figure S10).

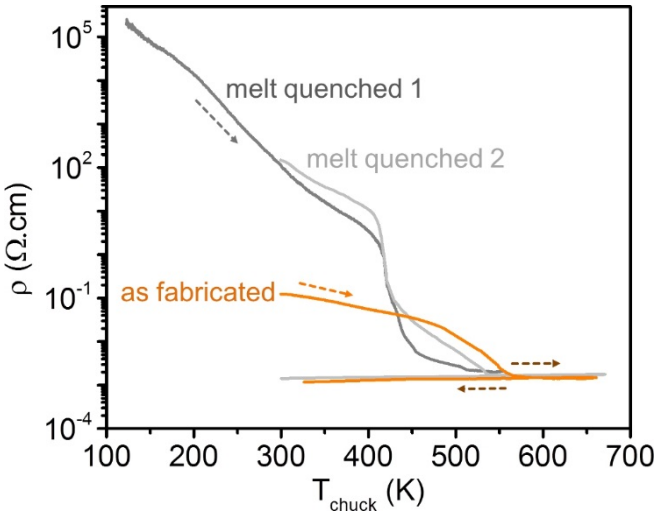

Figure S10. Measured GST resistivities as a function of temperature from slow *R-T* measurements (with 1-3.5 K/min heating rate) on three line cells.

Figure S11 summarizes the measurement procedure performed in this work.

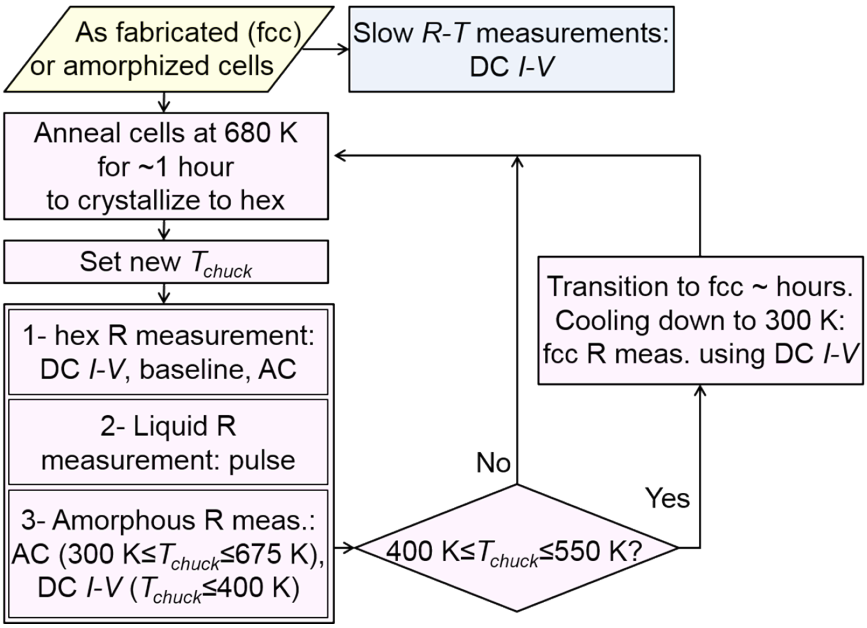

Figure S11. Flow chart depicting the measurement steps.

3. Modeling the Measurement Circuit

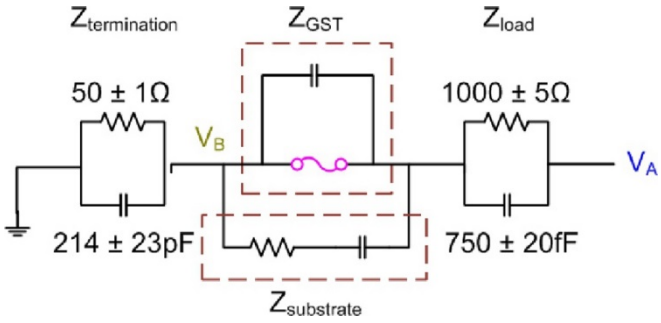

Figure S12. High-speed measurements circuit model.

Resistance values of GST line cells are calculated using the model shown in Figure S12. This model uses the circuit diagram shown in the main manuscript (Figure 1j), with the addition of capacitors associated with each circuit element. Inductance in the circuit elements and coaxial cables used in the experiments is negligibly small. The total complex impedance of the circuit is calculated using the voltage drop across the whole circuit (V_A) and termination impedance (V_B). Measurement errors in V_A and V_B are calculated using sinusoidal fit errors which are typically very small. Figure S13 shows measured V_B and V_A (with errors) on a GST line cell at 300 and 600 K. V_A and V_B values are provided in Table S1 for the 10th step (half maximum), showing very small errors in these voltage readings.

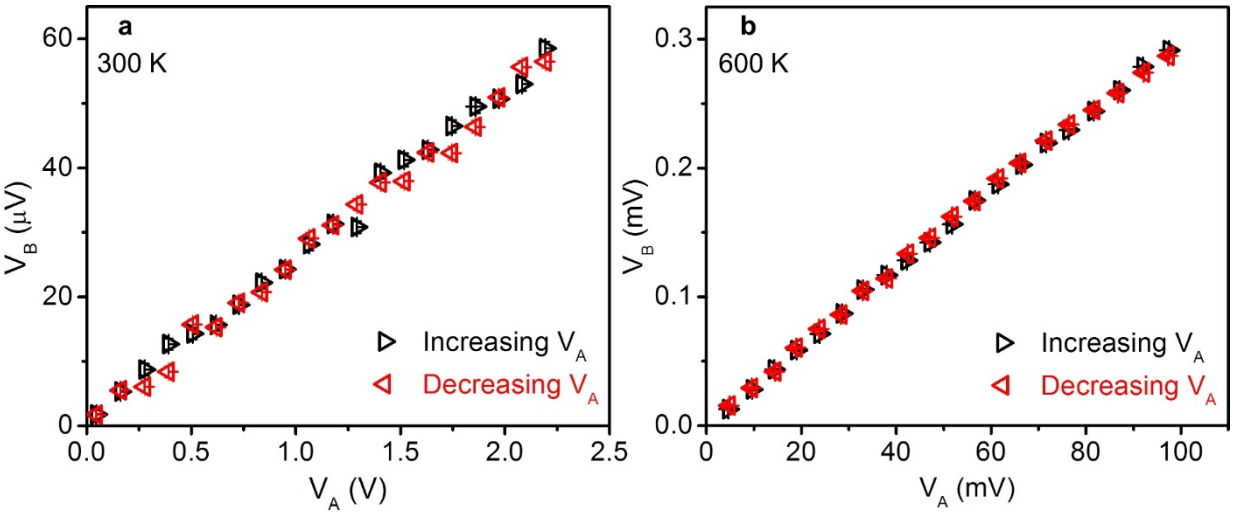

Figure S13. Example V_B versus V_A plots for a GST line cell during the 2 ms high-speed AC measurement (with increasing and decreasing sinusoidal signal amplitudes) following the melting pulse a) at 300 K and b) at 600 K.

Table S1. V_A and V_B values calculated using the sinusoid fits for the 10th step of the ac signals for the same examples in Figure S13.

	$T = 300$ K	$T = 600$ K
V_A	1.06 sin(ωt) (V)	(47.12 ± 0.08) sin(ωt) (mV)
V_B	(28.14 ± 0.94) sin(ω(t+190ns)) (μV)	(142.22 ± 0.73) sin(ω(t-2 ns)) (μV)

The phase difference between V_A and V_B readings is large (2π x 190 ns/1 μs) for low temperatures at which the substrate impedance, almost purely capacitive, dominates the current path. This large phase difference gives rise to a larger capacitive (imaginary) current reading compared to the resistive (real) current:

$$I\angle\phi_B - \phi_A = \frac{V_B\angle\phi_B - \phi_A}{Z_{\text{termination}}} \quad (1)$$

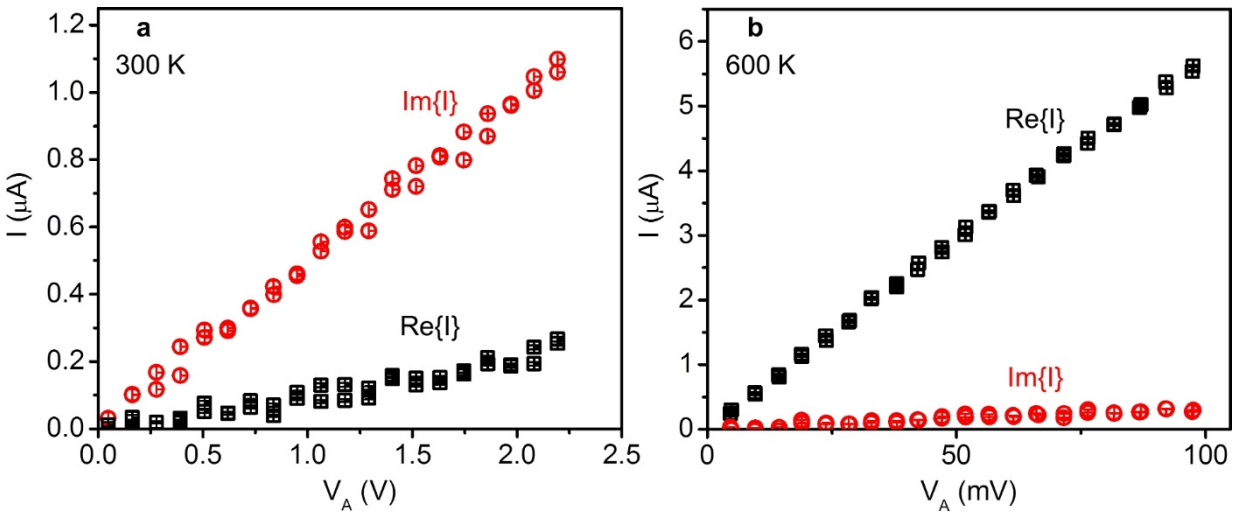

Figure S14. Real and imaginary components of current as functions of applied voltage (V_A) for a) 300 K and b) 600 K for the same examples in Figure S13.

Figure S14 shows corresponding imaginary and real current plots for 300 K and 600 K. The imaginary current is much larger than the real current at 300 K owing to the large GST line cell resistance, hence the large phase difference between V_B and V_A. The real component of current overwhelms the imaginary component at high temperatures. The total conductance of the circuit is found using slopes of linear regressions for I versus V_A curves. Errors in the

current, coming from the V_B readings, and uncertainties in the termination impedance are taken into account for the linear regressions. However, inclusion of these errors does not change the obtained conductance values, as these errors are very small (< 1%). The total impedance of the circuit is calculated using the imaginary and real components of the conductance values. Errors in the conductance values, coming from the linear regression process, are propagated to calculate the errors in the total impedance:

$$Z_{total} = \frac{1}{\mathrm{Re}\{\mathrm{Conductance}\} + j\ \mathrm{Im}\{\mathrm{Conductance}\}} \tag{2}$$

Table S2. Real and imaginary components of the total impedances for 300 K and 600 K for the same examples in Figure S13.

	***T* = 300 K**	***T* = 600 K**
$Z_{total\text{-}Real}$	0.43 ± 0.01 MΩ	17.27 ± 0.03 kΩ
$Z_{total\text{-}Imaginary}$	-1.97 ± 0.02 MΩ	-1.06 ± 0.00 kΩ

Table S2 shows calculated Z_{total} for the example GST line cell. Once Z_{total} is found the GST line cell impedance is calculated using known load, termination and substrate impedances:

$$Z_{GST} \,//\, Z_{substrate} = Z_{total} - Z_{load} - Z_{termination} \tag{3}$$

The substrate impedance ($Z_{substrate}$) and errors associated with it are measured on many broken wires using the same model at all chuck temperatures. An average value of (-370±50) kΩ + j (-4.8±0.1) MΩ is used for the calculations (Figure S15, Table S3). Although the real part of $Z_{substrate}$ is negative, results from the AC measurements using this model are close to the more reliable DC measurement results. The errors/uncertainties in these impedances are propagated to calculate the errors in GST cell impedance. A capacitor in parallel with the GST line cell is introduced in the model to account for any remaining complex component in the GST line cell impedance which is calculated to be typically small (< 1 pF). The errors in GST line cell impedance are dominated by the uncertainties in $Z_{substrate}$ as the

errors/uncertainties associated with the other circuit elements and measurements are very small. Table S4 shows the calculated resistance and capacitance for the same example GST line cell.

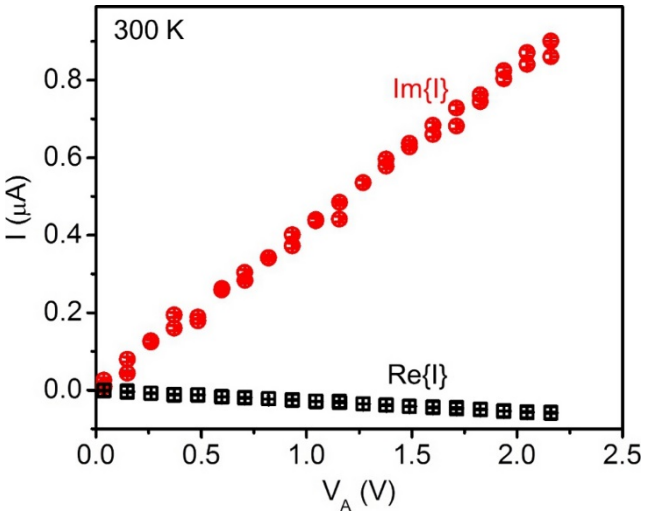

Figure S15. Real and imaginary components of current as functions of applied voltage (V_A) on a broken wire for 300 K.

Table S3. Real and imaginary components of the substrate impedance for 300 K for the same example in Figure S15.

	***T* = 300 K**
$Z_{substrate\text{-}Real}$	-0.37 ± 0.05 MΩ
$Z_{substrate\text{-}Imaginary}$	-4.8 ± 0.1 MΩ

The extracted total resistance (R_T) includes the GST line cell resistance (R_{GST}), contact resistance (R_X) (~98 Ω at 500 K), and metal extension resistance (R_M) (~200 Ω at 300 K and ~230 Ω at 675 K) (Eq. 4). Resistivity of GST line cells are calculated using the actual device dimensions length (*L),* width *(W),* and thickness *(t)* (Eq. 5).

$$R_T = R_{GST} + R_X + R_M \tag{4}$$

$$R_{GST} = \rho \frac{L}{Wt} \tag{5}$$

Table S4. Calculated resistances and capacitances for 300 K and 600 K for the same examples in Figure S13.

	***T* = 300 K**	***T* = 600 K**
R	7.7 ± 1.0 MΩ	16.3 ± 0.7 kΩ
C	16 ± 4 fF	570 ± 170 fF

We confirmed the accuracy of the AC high-speed measurement results by comparing them to highly sensitive DC *I-V* measurement results. It show that results from the AC high speed and DC *I-V* measurements are in good agreement GST line cell resistances up to ~100 MΩ using this model (Figure S16). Resistance of typical GST line cells used in AC high-speed measurements are in the order of 40 MΩ in the amorphous phase at room temperature. Very high resistance values (~100-400 MΩ) shown in Figure S16 are from the drifted GST line cells.

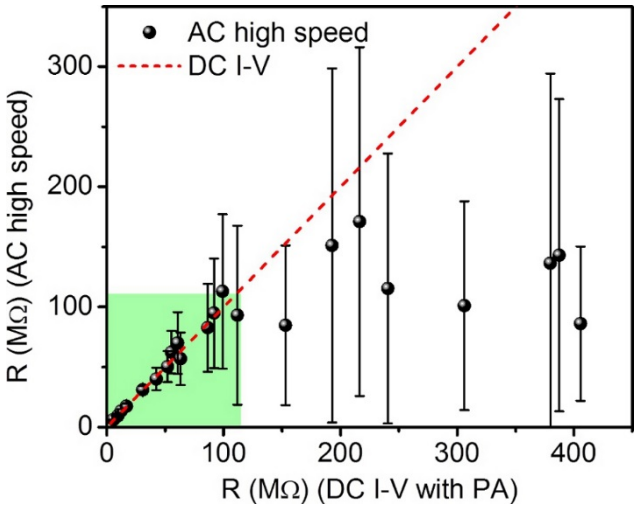

Figure S16. Comparison of AC high-speed measurement and DC *I-V* measurement results.

4. 4 MHz Measurements

4 MHz AC signals are used on a set of GST line cells to capture fast (~100 μs) amorphous to fcc transition at high temperatures (575-600 K) (Figure S17).

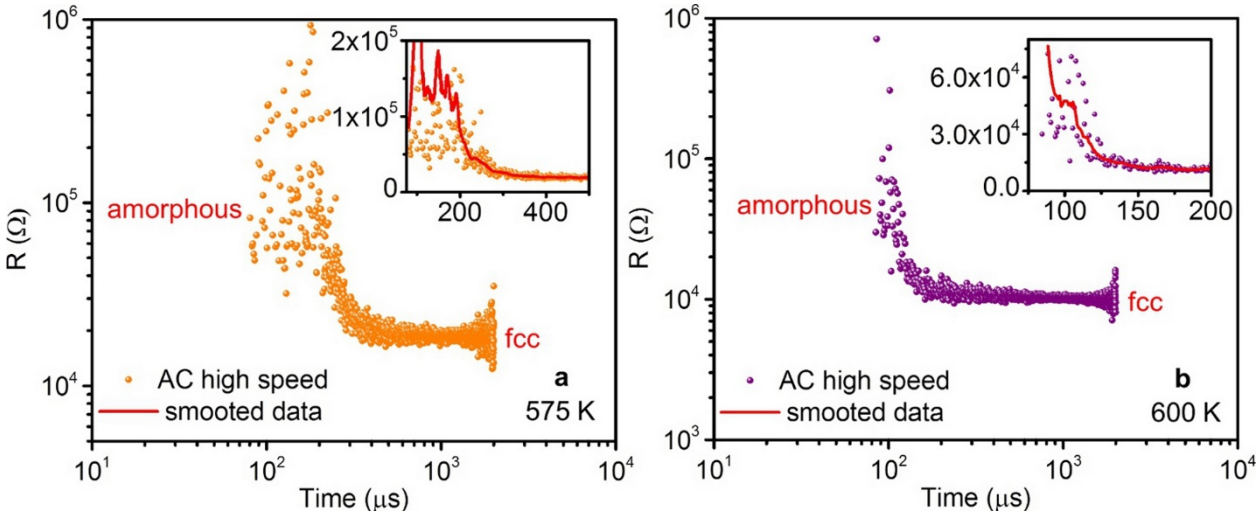

Figure S17. Example of 4 MHz AC high speed measurements performed a) at 575 K and b) at 600 K on GST line cells. Insets are the zoomed-in views of resistance change during amorphous to fcc transition (on the order of 100 μs). Amorphization pulse starts at 78 μs, followed by 1 μs 0 V cool-down period and AC signal starts at 80 μs.

The same measurements are performed at 450 K to observe the resistance drift behaviour in amorphous phase in 2 ms time range (Figure S18).

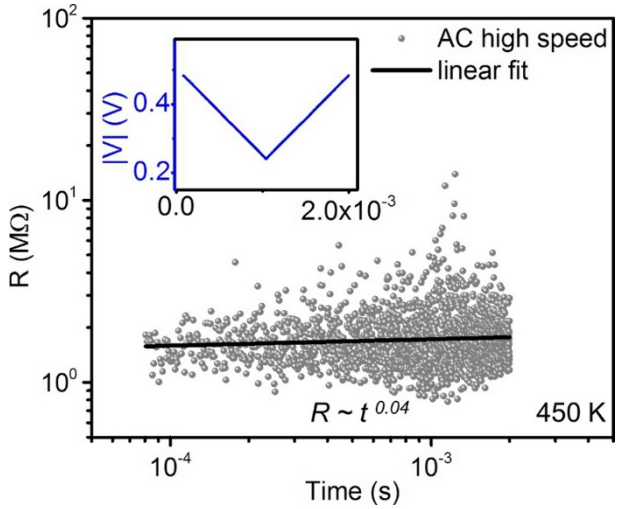

Figure S18. Resistance change (Drift) in amorphous phase at 450 K. Amorphization pulse starts at 78 μs, followed by 1 μs 0 V cool-down period and AC signal starts at 80 μs. Inset show the amplitudes of the sinusoids applied after the pulse.

5. Quasi Static Approach (DC High-speed Measurements)

We have performed DC high-speed measurements using a similar experimental setup. At lower temperatures ($T < 500$), DC high-speed measurements require a longer measurement duration (20 ms) -instead of 2 ms used for AC high-speed measurements- due to a longer *RC* time constant induced by the large termination resistance (1 MΩ) used to obtain readable current levels (Figure S19a). At higher temperatures ($T > 500$), a 50 Ω termination resistance is used due to lower cell resistances, enabling faster (2 ms) DC high-speed measurements (Figure S19b).

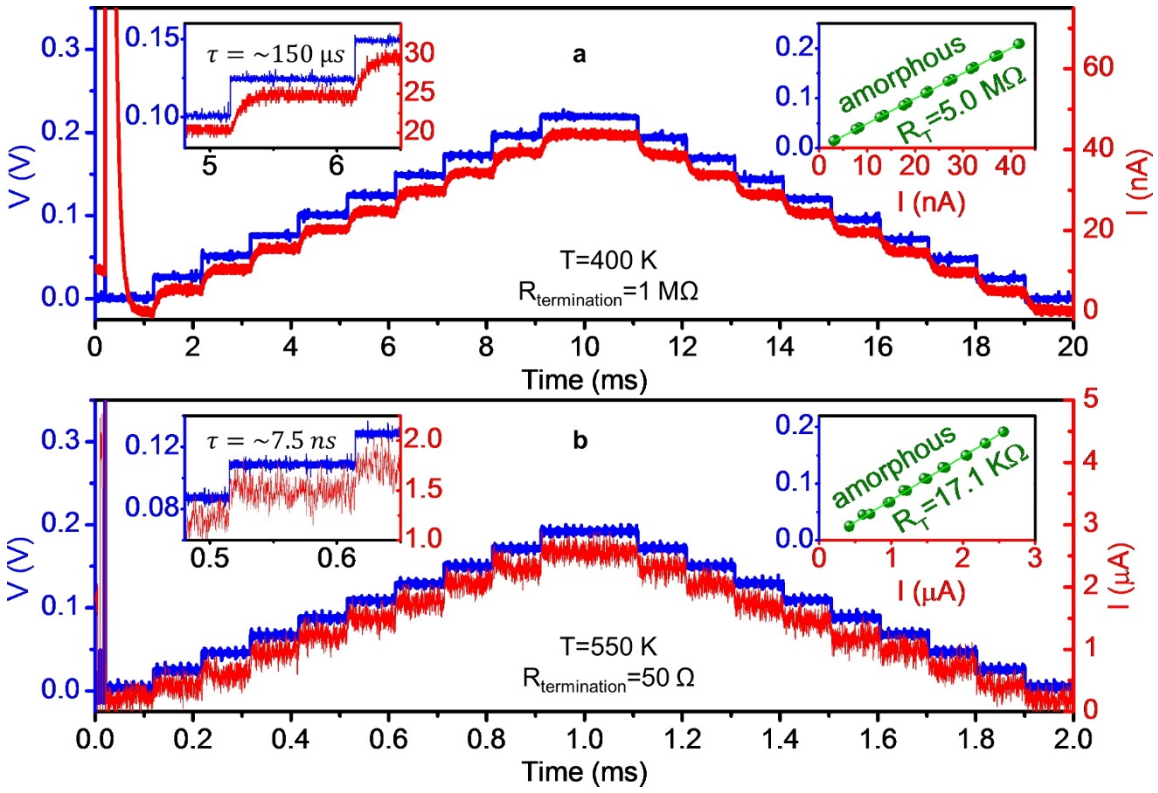

Figure S19. Example applied and measured signals showing voltage and current on amorphous GST line cells for the DC high-speed measurements a) at $T = 400$ K using 1 MΩ termination and b) at $T = 550$ K using 50 Ω termination. Insets show zoomed-in view of voltage and current for a DC signal step and *I-V* characteristics obtained from these measurements.

DC high-speed measurement results are in good agreement with those of DC *I-V* measurements at low temperatures and AC high-speed measurements at high temperatures (Figure S20).

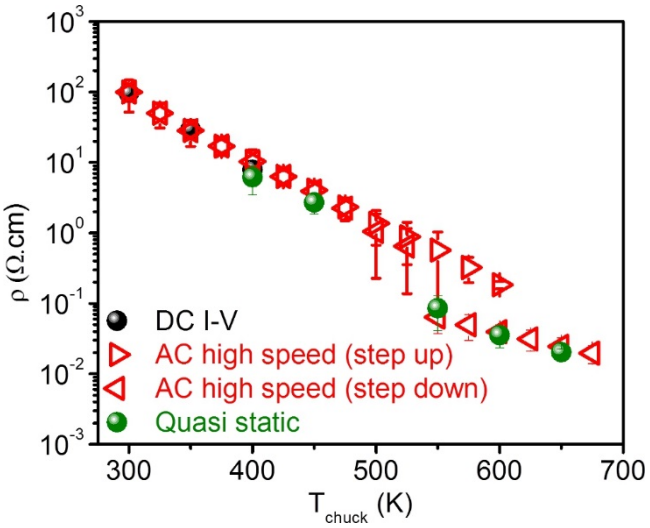

Figure S20. Comparison of the average amorphous GST resistivities measured using DC *I-V*, Quasi static approach, and AC high-speed measurement techniques.

6. Resistance Drift

The 26 devices measured for very long duration (~13 months) show a consistent trend in resistance drift at room temperature (~300 K). Their resistances have reached to maximum and turned around at ~4 months after the amorphization. The decrease in resistance after reaching the maximum is slower on wider structures (Figure S21).

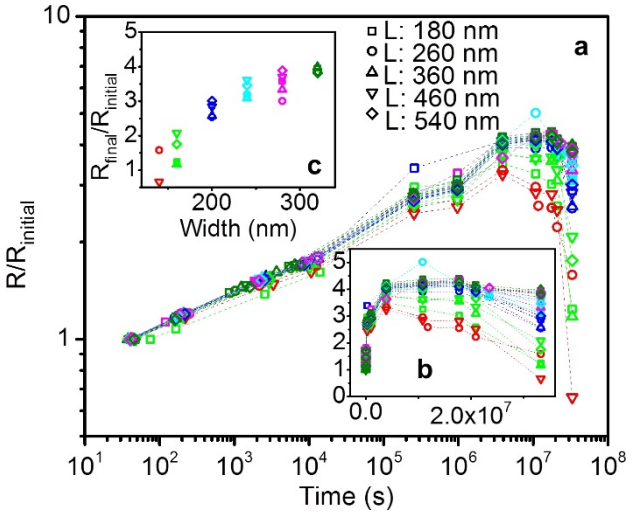

Figure S21. Normalized resistance as a function of time at 300 K in a) log and b) linear scales. c) $R_{final}/R_{initial}$ values as a function of device width for various lengths.

7. Electrical Resistivities of GST

AC high speed measurements are performed on 5 sets of devices. Each set consists of large number of devices (total of ~2000 measurements). Figure S22 shows distribution of all amorphous and crystalline (fcc) resistivities and average values from the AC high speed measurements compared to the slow *R-T* measurements.

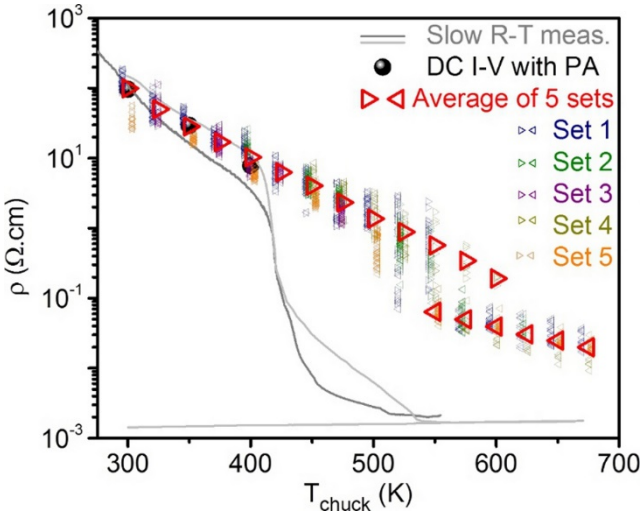

Figure S22. Measured amorphous and fcc GST resistivities using AC high speed measurements (small symbols are from high-speed measurements, large symbols are average of data collected from large number of line cells) and DC *I-V* measurements (solid symbols and lines are from standard slow *R-T* measurements (with 1-3.5 K/min heating rate) on two line cells).

Figure S23 shows distribution of all liquid resistivities and average values from the AC high speed measurements compared to other published data.

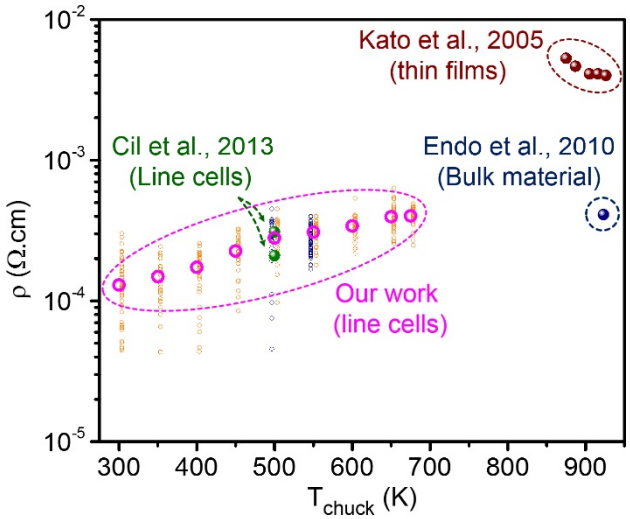

Figure S23. Measured liquid GST resistivities as a function of temperature (magenta open symbols). Reported liquid GST resistivities from thin films (wine solid symbols: Kato et al., 2005 (873-923 K)), from bulk material (navy solid symbol: Endo et al., 2010 (923 K)), from line cells (green solid symbols: Cil et al., 2013 (500 K)). Small symbols represent to individual measurements from our work.

Figure S24 and Table S5 shows average (from total of ~2000 measurements) resistivity values (liquid, crystalline (hexagonal and fcc), and amorphus) measured using all measurement techniques presented in this document.

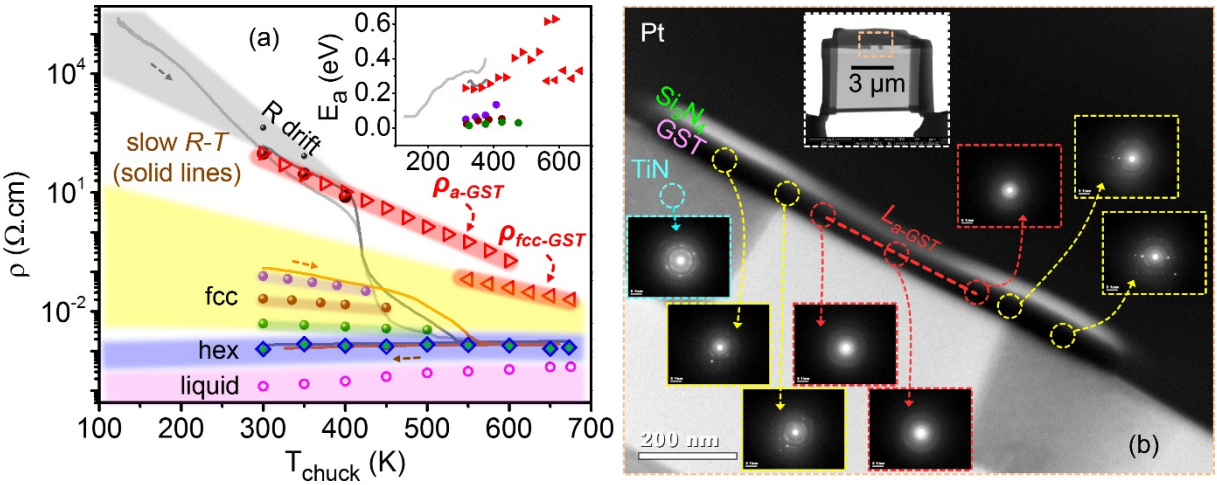

Figure S24. Temperature dependent electrical resistivity and activation energy of GST. a) Solid lines show standard slow *R-T* measurements (with 1-3.5 K/min heating rate) on three line cells. Symbols show measurement results at a constant chuck temperature (solid symbols are from DC measurements, open symbols are from high-speed measurements, open red triangles are metastable amorphous and fcc GST resistivities). Each data point is an average of data collected from large number of line cells. Inset shows calculated activation energies associated with carriers, with the corresponding colors and shapes. The direction of the triangles indicate the voltage stepping up (▷) and down (◁).b) TEM (Transmission electron microscopy) and SADP (Selected area diffraction pattern) images of a sample (design *L*: 340 nm, *W*: 120 nm) measured device. SADP images show crystal pattern on top the contacts and amorphous pattern around the center of the line cell, that verify amorphization occurs on the narrower section of the structure and dominates the measured resistance.

Table S5. Measured liquid, crystalline (hexagonal and fcc), and amorphous GST resistivity values.

Phase		Liquid GST		Crystalline (hexagonal) GST				Crystalline (fcc) GST					Amorphous GST				
Technique		During the pulse						Annealed @ 425 K	Annealed @ 450 K	Annealed @ 500 K				Stepping up		Stepping down	
		AC high-speed		DC *I-V*	baseline	AC high-speed		DC *I-V*			AC high speed		DC *I-V*	AC high-speed			
		ρ	±	*P*	ρ	ρ	±	ρ	ρ	ρ	ρ	±	ρ	ρ	±	ρ	±
		(μΩ.cm)		(μΩ.cm)				(mΩ.cm)					(mΩ.cm)				
Temperature (K)	300	130.0	63.2	1020.0	1150.0	1130.0	663.2	78.2	21.1	5.0			96439.3	99512.8	47620.7	99690.3	47936.6
	325													50086.6	19379.9	50031.9	19026.9
	330							65.7									
	335								19.2								
	350	149.0	41.1	1350.0	1460.0	1500.0	486.6			4.6			29247.0	28336.7	11467.9	28279.1	11303.3
	360							54.6									
	370								16.7								
	375													16946.9	3931.3	17136.3	4424
	390							45.4									
	400	173.8	42.8	1220.0	1360.0	1360.0	534.1		14.9	4.1			7867.5	10330.1	4772.8	10293.8	4812.1
	425							32.6						6288.9	1407.1	6317.9	1579.5
	450	226.3	64.1	1330.0	1420.0	1300.0	372.8		12.5	3.7				4035.5	1392.1	3907.3	1371.6
	475													2333.5	793.5	2237.6	742.9
	500	280.2	82.7	1340.0	1460.0	1470.0	412.7			3.6				1367.4	699.3	1050.6	823.0
	525													884.5	528.1	649.7	512.2
	550	308.8	51.0	1250.0	1380.0	1430.0	343.5				63.8	26.5		568.8	462.9		
	575										49.7	19.8		324.0	127.0		
	600	341.3	61.1	1220.0	1310.0	1370.0	355.1				39.4	10.3		191.0	16.2		
	625										31.3	10.4					
	650	396.6	86.7	1130.0	1160.0	1150.0	237.0				24.6	7.7					
	675	402.4	65.1	1210.0	1220.0	1230.0	373.1				19.7	5.6					